Journal of Visualized Experiments

Optical Tweezers to Study RNA-Protein Interactions in Translation Regulation

--Manuscript Draft--

Article Type:	Invited Results Article - Author Produced Video
Manuscript Number:	JoVE62589R2
Full Title:	Optical Tweezers to Study RNA-Protein Interactions in Translation Regulation
Corresponding Author:	Neva Caliskan Helmholtz Institute for RNA-based Infection Research: Helmholtz-Institut fur RNA-basierte Infektionsforschung Würzburg, Bayern GERMANY
Corresponding Author's Institution:	Helmholtz Institute for RNA-based Infection Research: Helmholtz-Institut fur RNA-basierte Infektionsforschung
Corresponding Author E-Mail:	neva.caliskan@helmholtz-hiri.de
Order of Authors:	Lukas Pekarek
	Stefan Buck
	Neva Caliskan
Additional Information:	
Question	**Response**
Please indicate whether this article will be Standard Access or Open Access.	Standard Access (US$1200)
Please specify the section of the submitted manuscript.	Biochemistry
Please confirm that you have read and agree to the terms and conditions of the author license agreement that applies below:	I agree to the Author License Agreement
Please provide any comments to the journal here.	
Please indicate whether this article will be Standard Access or Open Access.	Standard Access ($1400)
Please confirm that you have read and agree to the terms and conditions of the video release that applies below:	I agree to the Video Release

TITLE:

Optical Tweezers to Study RNA-Protein Interactions in Translation Regulation

AUTHORS AND AFFILIATIONS:

Lukas Pekarek[1], Stefan Buck[1], Neva Caliskan[1,2]

[1]Helmholtz Institute for RNA-based Infection Research (HIRI), Helmholtz Zentrum für Infektionsforschung (Helmholtz Centre for Infection Research), Würzburg, Germany

[2]Medical Faculty, Julius-Maximilians University Würzburg, Würzburg, Germany

Email Addresses of Co-Authors:

Lukas Pekarek (Lukas.Pekarek@helmholtz-hiri.de)

Stefan Buck (Stefan.Buck@helmholtz-hiri.de)

Neva Caliskan (Neva.Caliskan@helmholtz-hiri.de)

Corresponding author:

Neva Caliskan (Neva.Caliskan@helmholtz-hiri.de)

SUMMARY:

This protocol presents a complete experimental workflow for studying RNA-protein interactions using optical tweezers. Several possible experimental setups are outlined including the combination of optical tweezers with confocal microscopy.

ABSTRACT:

RNA adopts diverse structural folds, which are essential for its functions and thereby can impact diverse processes in the cell. In addition, the structure and function of an RNA can be modulated by various *trans*-acting factors, such as proteins, metabolites or other RNAs. Frameshifting RNA molecules, for instance, are regulatory RNAs located in coding regions, which direct translating ribosomes into an alternative open reading frame, and thereby act as gene switches. They may also adopt different folds after binding to proteins or other trans-factors. To dissect the role of RNA-binding proteins in translation and how they modulate RNA structure and stability, it is crucial to study the interplay and mechanical features of these RNA-protein complexes simultaneously. This work illustrates how to employ single-molecule-fluorescence-coupled optical tweezers to explore the conformational and thermodynamic landscape of RNA-protein complexes at a high resolution. As an example, the interaction of the SARS-CoV-2 programmed ribosomal frameshifting element with the *trans*-acting factor zinc-finger antiviral protein (ZAP) is elaborated. In addition, fluorescence-labeled ribosomes were monitored using the confocal unit, which would ultimately enable the study of translation elongation. The fluorescence coupled OT assay can be widely applied to explore diverse RNA-protein complexes or trans-acting factors regulating translation and could facilitate studies of RNA-based gene regulation.

INTRODUCTION:

Transfer of genetic information from DNA to proteins through mRNAs is a complex biochemical process, which is precisely regulated on all levels through macromolecular interactions inside cells. For translational regulation, RNA-protein interactions confer a critical role to rapidly react to various stimuli and signals[1,2]. Some RNA-protein interactions affect mRNA stability and thereby alter the time an RNA is translationally active. Other RNA-protein interactions are associated with recoding mechanisms such as stop-codon readthrough, bypassing, or programmed ribosomal frameshifting (PRF)[3-7]. Recently, a number of RNA-binding proteins (RBPs) have been demonstrated to interact with stimulatory mRNA elements and the translation machinery to dictate when and how much recoding will occur in the cell[7-11]. Thus, to dissect the role of RNA-binding proteins in translation and how they modulate RNA structure and stability, it is pivotal to study the interaction principles and mechanical properties of these RNA-protein complexes in detail.

Decades of work have laid the foundation to study the multi-step and multi-component process of translation, which relies on intricate communication between the RNA and protein components of the translation machinery to achieve speed and accuracy[12-14]. A crucial next step in understanding complex regulatory events is determining the forces, timescales, and structural determinants during translation at high precision[12,15-17]. The study of RNA conformational dynamics and especially how *trans*-acting auxiliary factors act on the RNA structure during translation have been further illuminated by the emergence of single-molecule tools, including optical tweezers or zero-mode waveguides[16-26].

Optical tweezers (OT) represent a highly precise single-molecule technique, which has been applied to study many sorts of RNA-dependent dynamic processes including transcription, and translation[26-32]. The use of optical tweezers has allowed probing of molecular interactions, nucleic acid structures, and thermodynamic properties, kinetics, and energetics of these processes in detail[16,17,22,33-39]. Optical tweezers assay is based on the entrapment of microscopic objects with a focused laser beam. In a typical OT experiment, the molecule of interest is tethered between two transparent (usually polystyrene) beads (**Figure 1A**)[27]. These beads are then caught by optical traps, which behave like springs. Thus, the force applied on the molecule can be calculated based on the bead's displacement from the center of the focused laser beam (trap center). Recently, optical tweezers have been combined with confocal microscopy (**Figure 1B**), enabling fluorescence or Förster resonance energy transfer (FRET) measurements[40-42]. This opens a whole new field of possible experiments allowing simultaneous measurement and, therefore, precise correlation of force spectroscopy and fluorescence data.

Here, we demonstrate experiments using the optical tweezers combined with confocal microscopy to study protein-RNA interactions regulating translational frameshifting. Between the objective and the condenser, a flow cell with five channels enables continuous sample application with laminar flow. Through the microfluidic channels, various components can be injected directly, which decreases the hands-on time as well as allowing very little sample consumption throughout the experiment.

First, a basic guideline to assist the design of OT experiments is proposed and advantages as well as pitfalls of various setups are discussed. Next, the preparation of samples and experimental workflows are described, and a protocol for the data analysis is provided. To represent an example, we outline the results obtained from RNA stretching experiments to study the SARS-CoV-2 frameshifting RNA element (**Figure 2A**) with the *trans*-acting factor zinc-finger antiviral protein (ZAP), which alters the translation of the viral RNA from an alternative reading frame[43]. Additionally, it is demonstrated that fluorescence-labeled ribosomes can be employed in this OT confocal assay, which would be useful to monitor the processivity and speed of the translation machinery. The method presented here can be used to rapidly test the effect of different buffers, ligands, or other cellular components to study various aspects of translation. Finally, common experimental pitfalls and how to troubleshoot them are discussed. Below, some crucial points in experimental design are outlined.

Construct design

In principle, there are two common approaches to create an OT-compatible RNA construct. The first approach employs a long RNA molecule that is hybridized with complementary DNA handles, thus yielding a construct consisting of two RNA/DNA hybrid regions flanking a single-stranded RNA sequence in the middle (**Figure 2B**). This approach is employed in most OT RNA experiments[33,44,45].

The second approach takes advantage of dsDNA handles with short (around 20 nt) overhangs[15,17]. These overhangs are then hybridized with the RNA molecule. Although more complicated in design, the use of dsDNA handles overcomes some of limitations of the DNA/RNA-hybrid system. In principle, even very long handles (>10kb) can be implemented, which is more convenient for confocal measurements. In addition, the RNA molecule can be ligated to DNA handles to increase tether stability.

End-labeling strategy

The construct must be tethered to beads via a strong molecular interaction. While there are approaches available for covalent bonding of handles to beads[46], strong but non-covalent interactions such as streptavidin-biotin and digoxigenin-antibody are commonly used in OT experiments[15,33,35,45]. In the described protocol, the construct is labeled with biotin or digoxigenin, and the beads are coated with streptavidin or antibodies against digoxigenin, respectively (**Figure 1A**). This approach would be suitable for applying forces up to approximately 60 pN (per tether)[47]. Furthermore, the use of different 5’ and 3’ labeling strategies allow determining the orientation of the tether formed between the beads[17].

Protein labeling for fluorescence measurements

For the confocal imaging, there are several commonly used approaches for fluorescence labeling. For instance, fluorophores can be covalently attached to amino acid residues that are found natively in proteins or introduced by site-directed mutagenesis through a reactive organic group. Thiol or amine-reactive dyes can be used for labeling of cysteine and lysine residues, respectively. There are several reversible protection methods to increase the specificity of labeling[48,49], however native proteins would typically be labeled at multiple residues. Although the small size of the fluorophore may confer an advantage, non-specific labeling might interfere with the protein activity and thus signal intensity may vary[49]. Also, depending on the labeling efficiency signal intensity may differ between different experiments. Therefore, an activity check should be performed prior to the experiment.

In case the protein of interest contains an N- or C-terminal tag, such as a His-tag or strep-tag, specific labeling of these tags represents another popular approach. Moreover, tag-targeted labeling reduces the chance of the fluorophore interfering with protein activity and can enhance solubility[49]. However, tag-specific labeling usually yields mono-fluorophore labeled proteins, which might be challenging to detect. Another way of specific labeling can be accomplished by employing antibodies.

Microfluidics setup

The combination of OT with a microfluidics system allows a rapid transition between different experimental conditions. Moreover, current systems take advantage of maintaining the laminar flow inside the flow cell, which precludes the mixing of liquids from other channels in the perpendicular direction relative to the flow direction. Therefore, laminar flow is particularly advantageous for the experimental design. Currently, flow cells with up to 5 channels are commonly employed **(Figure 3**).

PROTOCOL:

1. **Sample preparation**

1.1. Clone the sequence of interest into the vector containing the Lambda DNA fragments, which serves as the handle sequences (**Figure 2**)[43,50].

1.2. First generate a DNA template for subsequent *in vitro* transcription via PCR (**Figure 2B**; reaction 1). At this PCR step, the T7 promoter is added in the 5' end of the sense DNA molecule[32,33,43,50]. Set the PCR reaction according to **Table 1**. Run the PCR in 50 µL aliquots with appropriate cycles in the thermocycler.

1.3. Prepare the handles by two separate PCR reactions (**Table 1**, **Figure 2B**; reaction 2 and 3). First, generate the 5’ handle by PCR. Then, generate the 3' handle and simultaneously label it with digoxigenin by using a 5' digoxigenin-labeled primer[32,33,43,50].

1.4. After the PCR, purify the DNA using silica spin columns.

1.5. Carry out the *in vitro* transcription reaction using T7 RNA polymerase (**Table 2**)[32,33,43,50]. Incubate the reaction at 37 °C for 2-4 h depending on the length of the RNA. Next, add DNase I to the reaction and incubate at 37 °C for 30 min to digest the DNA template. Purify the RNA using silica spin columns.

1.6. During the labeling reaction of the 5’ handle (**Table 3**), add biotin-16-dUTP at the 3' end of the handle by T4 DNA polymerase[38,50]. Perform the reaction at room temperature for 1-2 h. Afterwards, purify the DNA using silica spin columns.

NOTE: Since the 5' handle must be labeled at its 3' end (**Figure 2B**), the labeling cannot be performed during the PCR.

1.7. Mix the components mentioned above – 5' handle (3' labeled with biotin), 3' handle (5' labeled with digoxigenin), and RNA – in a 1:1:1 molar ratio in annealing buffer (80% formamide, 400 mM NaCl, 40 mM HEPES, pH 7.5, 0.5 mM EDTA, pH 8), to obtain the desired RNA/DNA hybrid (**Table 4**). Heat the annealing mixture up to 85 °C for 10 min and then slowly cool down to 4 °C.

1.8. Mix the annealed sample with 1/10 of volume of 3 M sodium acetate (pH 5), 3 volumes of ice-cold ethanol and incubate at -80 °C for at least 1 h or at -20 °C overnight.

1.9. Centrifuge the samples at 15,000 × *g* for 30 min at 4 °C. Discard the supernatant and dry the pellet (usually not visible) under vacuum.

1.10. Finally, resuspend, the pellet in 50 µL of RNase-free water and make aliquots. Store the aliquots at -80 °C until used. For short term storage, the samples can be also stored at -20 °C.

2. Instrument setup

NOTE: The following protocol is optimized for the commercial optical tweezers instrument C-Trap from LUMICKS company. Therefore, adjustments to the presented steps might be necessary while using other optical tweezers instruments. If not used, the microfluidics system of the machine is kept in bleach (sodium hypochlorite solution) and must be washed before use.

2.1. Discard the bleach and fill the syringes with 1 mL of RNase-free water.

2.2. Add 50 µL of 0.5 M sodium thiosulfate to at least 1 mL of the RNase-free water and thoroughly wash the system (1 bar, at least 0.5 mL) to eliminate the remaining bleach in the system.

2.3. Discard the sodium thiosulfate solution from the syringes. Replace syringes with fresh ones and wash the system with at least 0.5 mL of RNase-free water.

NOTE: Be careful, that the microfluidics system never runs dry to avoid air bubbles in the system.

2.4. Put 2 drops of immersion oil (refractive index of 1.33) or approximately 70 µL of water on top of the objective.

2.5. Place the flow cell inside the holding frame in its position.

2.6. Put 2 drops of immersion oil (refractive index of 1.51) on top of the flow cell.

2.7. Turn on the laser device in the tweezers machine. Once it is running, turn on the trapping laser in the software interface at 100%.

2.8. Using diagnostic cameras (Z finder), adjust the Z-axis to the middle of the chamber between the second and the third reflections (interfaces) where the refraction rings are the biggest, by turning the micro screw.

NOTE: Each time the objective is moved closer to the measuring chamber and the focal plane of the objective crosses the interface between two phases, a reflection can be recognized in the Z-finder mode. There are 4 interfaces possible: (i) water/immersion oil and bottom glass (ii) bottom glass and buffer inside the chamber (iii) buffer inside the chamber and top glass (iv) top glass and immersion oil for condenser.

2.9. Adjust the condenser position (set trapping laser to approximately 50%) so the condenser touches the immersion oil on top of the measuring chamber.

2.10. Adjust the focus by moving slowly down/up with the condenser, so approx. 10 light bands are shown in the moon mode (diagnostic cameras).

3. Sample measurement

3.1. Incubate anti-digoxigenin-coated beads (AD) with the sample constructs (3 µL of 0.1% (w/v) AD bead suspension + 4 µL of sample) and with 1 µL of RNase inhibitors and 8 µL of the assay buffer (300 mM KCl, 5 mM $MgCl_2$, 20 mM HEPES, pH 7.6, 0.05% Tween 20, 5 mM DTT) at RT for 10-20 min. After the incubation, dilute the sample in 500 µL of assay buffer.

NOTE: It is recommended to add oxygen scavengers, particularly during fluorescence measurements to the buffer in order to prevent oxidative damage. Here oxygen scavenger system containing glucose (8.3 mg/mL), glucose oxidase (40 U/mL) and catalase (185 U/mL) was used.

3.2. Mix 0.8 µL of 1% (w/v) streptavidin-coated (SA) beads with 1 mL of assay buffer.

3.3. Discard water from the syringes and fill the syringes with respective suspensions/solutions. Wash for at least 2 min at approximately 1 bar, and then start catching beads.

NOTE: Depending on the experimental set-up, different channel arrangements may be used (**Figure 3**). Typically, one flow channel is filled with anti-digoxigenin beads carrying the RNA molecule. A second channel is filled with the streptavidin-coated beads. Buffer channel is used to form the tethers (**Figure 3B**). A fourth channel can be employed to load the RNA binding protein, or alternatively RBP can be added directly in the buffer channel (**Figure 3C**).

3.4. To capture the beads, move the optical traps apart from each other. First move to the AD channel and catch an AD-bead in trap 1. Next, move the stage to the SA-channel and catch a single SA bead by trap 2.

NOTE: Try to stay at the interface of the buffer and bead channels to avoid losing the already caught bead, or to prevent catching multiple beads by the same trap.

3.5. Once the beads of the right size are captured, move to the buffer channel and stop the laminar flow. Next, perform force calibration to check trap stiffness. The respective stiffness values should not differ in the x/y axis by more than 10-15%.

NOTE: Adjust the laser power or the laser split between the traps according to bead size. Force calibration does not have to be done for every bead pair as long as the bead templates match (similarity score > 0.9). However, it should be performed regularly, or at least every time assay conditions are changed.

3.6. Start fishing for a tether by moving the beads close to each other, waiting for a few seconds, and then moving them back apart, repeat until a tether is formed. A tether formation results in an increase of measured force upon pulling the two beads away from each other.

NOTE: To avoid formation of multiple tethers, the beads should not be moved too close. Upon catching a tether between the two beads, tether quality can be checked by finding the overstretching plateau. The plateau should be between 50 to 60 pN for a single tether.

3.7. Upon obtaining a tether, start the measurement. Depending on the phenomenon studied different measurement setups should be chosen (**Figure 1B-D**).

NOTE: Usually at the beginning of the experiment, a force-ramp experiment is conducted to check the tether quality and probe the behavior. Afterward, one may also start the constant-force or constant-position experiments to study the state transitions further. Once sufficient number of measurements have been performed on an RNA sample to determine its behavior, labeled factors can be added to the system to perform confocal measurements.

3.8. To perform fluorescence measurements, turn on the confocal lasers and photon counter unit in the optical tweezers instrument.

3.9. Turn on the excitation laser of desired wavelength in the software interface and set the power of the laser to 5% or higher, depending on the fluorophore.

NOTE: While not measuring lower the power setting of the excitation laser to 0% to avoid excessive photodamage to the sample.

3.10. Start imaging the sample by using image functions of the software.

NOTE: In order to get well-focused images, the focal plane of the confocal microscope and optical traps have to be aligned. For this purpose, autofluorescence of the polystyrene beads in the blue laser channel can be employed. The focal plane of optical traps is moved up or down in the z-axis until the image of beads reaches its highest diameter. At this position, the fluorescence signal from the molecule tethered between the beads can be measured.

3.11. To use the kymograph function, specify the x-y position of the kymograph axis so that it allows detection of the tether between the beads.

3.12. Throughout the measurement, buffer composition can be easily changed by either moving the beads to different channels or by changing the buffer supplied in the microfluidics system.

4. **Data analysis**

4.1. Raw data pre-processing

4.1.1. By using a simple script, downsample the data (**Figure 4A**) enough to (**i**) allow faster subsequent data processing but (**ii**) still contain all the critical information. Usually, 100-5000 Hz is suitable for this purpose.

NOTE: The data gathering frequency in optical tweezers experiments is often higher than it is necessary for the analysis – in the presented experiments, the data gathering frequency is set to 78 125 Hz by default. Since storage space is limited, it is convenient and timesaving to reduce the sampling rate of the data. Here, the raw data were downsampled by a factor of 30.

4.1.2. Next, employ a signal filter to reduce the high frequency measurement noise from the signal (**Figure 4A**). Adjust the filter degree and cut-off frequency parameters accordingly to optimize data output of different experiments (**Figure 5**).

NOTE: Amongst signal filters, Butterworth filter[51] is one of the most widely used. A custom-written python script allowing the pre-processing of raw data is provided in the supplementary data. Downsampling and signal filtering parameters (cut-off frequency, filter degree) need to be optimized for different experiments.

4.2. For force-ramp data analysis, use the following steps.

4.2.1. Mark the steps either manually by finding corresponding points on the force trajectory plot or by using custom-written scripts. Unfolding steps are characterized by a sudden drop in force combined with an increase in distance in the force-distance (FD) curve.

4.2.2. Once unfolding events are marked, fit different regions of the FD curve using appropriate models (**Figure 4D**).

NOTE: For the region before the first unfolding step, the tether can be considered "double-stranded" and is commonly fit using an extensible Worm-like-chain model (WLC)[47,52,53]. The parts after the first unfolding event are considered a combination of double-stranded nucleotides (handles) and single-stranded nucleotides (unfolded RNA molecule). Therefore, the fit is more complex – usually a combination of 2 WLC models or WLC and Freely-jointed chain (FJC) models[36,39,52]. The extensible WLC model has two main fit parameters the contour length (L_C) and the persistence length (L_P). Contour length corresponds to the length of the fully stretched molecule and persistence length defines the bending properties of the molecule of interest. The model can be described with the following equation (1). WLC can be used to model the behavior of both folded as well as unfolded regions, although for each of these a separate model with different parameters has to be employed.

$$(1) \qquad x_{WLC} = L_C\left[1 - \frac{1}{2}\left(\frac{k_B T}{F \cdot L_P}\right)^{1/2} + \frac{F}{S}\right]$$

where x is extension, L_C is contour length, F is force, L_P is persistence length, k_B is Boltzmann constant, T is Thermodynamic temperature, and S is stretch modulus.

The second model called Freely-jointed chain (FJC) is commonly used to describe behavior of unfolded single stranded regions. It uses similar parameters of the polymers but treats each unit of the “chain” as a rigid rod, here corresponding to the nucleotides of the unfolded single stranded region. The following equation (2) describes this model:

$$(2) \qquad x_{FJC} = L_C\left[\coth\left(\frac{2F \cdot L_P}{k_B T}\right) - \frac{k_B T}{2F \cdot L_P}\right]\left(1 + \frac{F}{S}\right)$$

NOTE: Our lab has recently developed an algorithm that allows batch processing of the raw force-ramp data called Practical Optical Tweezers Analysis TOol (POTATO)[54]. The algorithm downsamples and filters the data, then it identifies possible unfolding steps and finally performs data fitting. The POTATO is built in a user-friendly graphical user interface (GUI) (https://github.com/REMI-HIRI/POTATO).

4.3. Process constant-force data as follows:

NOTE: The following instructions can be analogically applied on constant-position data.

4.3.1. For the constant-force data, plot the distance over time (**Figure 5**). A histogram showing the frequency (counts) of different conformations over the relative change in position is a useful way to characterize various dominant and minor states (**Figure 7**).

4.3.2. Fit the histogram using (multiple) Gaussian functions to estimate the overall percentage of individual conformers at a given force (**Figure 7C**). The Gaussian fits, mean position, and the standard deviation outlines the force-related relationship among different populations.

NOTE: A custom-written python script allowing pre-processing and basic bimodal Gaussian fitting of constant-force data is provided in the supplementary data. Parameters (cut-off frequency, filter degree, expected means, standard deviation values and amplitudes) need to be optimized for different experiments.

4.3.3. Next, employ the Hidden Markov model to further analyze the states, which may uncover additional folding intermediates (conformers)[55]. For further information on the constant-force and Hidden Markov model, one may refer to[55-58].

REPRESENTATIVE RESULTS:

In this section, focus is mainly given on measurements of RNA-protein/ligand interactions by the fluorescence optical tweezers. For a description of general RNA optical tweezers experiments and corresponding representative results, see[32]. For more detailed discussion of the RNA/DNA-protein interactions, also see[1,2,26,59,60].

In principle, binding of an RBP or any other trans-acting factor of interest on the RNA stabilizes, destabilizes, or may alter the conformation of the molecule. Below, a depiction of the mechanical observables for each effect are shown. However, the actual effect observed for a given RNA-protein complex is not limited to these below-mentioned scenarios.

Stabilization

The RNA structure can be specifically recognized and bound by the protein or other ligands[45,61-64]. The formation of the bonds is accompanied by a release of energy. Therefore, an extra energetical barrier must be overcome in order to unfold the given RNA structure. As a result, an increase in the mean unfolding force might be observed[50,65]. The stabilization of the RNA structure by binding of an external agent (protein, small molecule, other trans-acting factors) may also result in a change of the folding kinetics of the structure[45]. For that, further measurements can be performed in the constant-force mode, where less frequent transitions between the folding intermediates as well as force-shift in the equilibrium can be observed.

Destabilization

Some proteins recognize certain sequence motifs rather than specific RNA structures. The binding sites may vary from a highly specific motif to a more general pattern such as GC or AU rich stretches[60,66]. Nevertheless, if the protein preferentially binds to the unfolded single-stranded RNA conformation, the equilibrium between the folded and unfolded state can be shifted towards the unfolded state[36,43,67]. In **Figure 6** and **Figure 7** examples of such behavior are depicted.

Structure alteration

In some instances, RBPs (or other ligands) might combine both mechanisms mentioned above in such a way that the RBP destabilizes the previously dominant conformation and shifts the equilibrium towards an alternative RNA structure[44,68,69]. The switch to an alternative state may result in a change in the observed conformational population frequencies as well as the occurrence or disappearance of individual folding states. These changes can be first observed in force-ramp experiments and can be further investigated by the constant-force (or constant-position) experiments.

Effect of the *trans*-acting factor on RNA folding/unfolding

Here, an RNA sequence corresponding to the -1 programmed ribosomal frameshifting element of SARS-CoV-2 was studied. This RNA element is predicted to form an H-type pseudoknot[70,71]. In the example force-distance trajectories, the RNA unfolds and refolds in two consecutive steps (**Figure 6A**). These two steps likely correspond to the two stem loops that are the prerequisite for the pseudoknot formation. In this case, the pseudoknot was not observed either because the RNA did not fully fold or formed an alternative structure competing with the pseudoknot. Upon addition of the *trans*-acting factor ZAP, a sudden disappearance of the refolding events and a huge hysteresis was observed (**Figure 6B**)[43]. This suggests that the protein binds to the single-stranded state of the RNA, impeding the formation of secondary structures. Furthermore, constant-force experiments confirm the results of force-ramp experiments. Accordingly, while the RNA is fully folded at around 10 pN, the presence of the protein shifts the refolding towards lower forces, and at 10 pN the RNA is still mostly occupying the unfolded state (**Figure 7**).

OT measurements coupled with confocal microscopy

Next, exemplary results are shown for the non-specific as well as specific binding of different fluorophores and labeled ribosomes (**Figure 8**). In the first example, Sytox dye was used to label the tethered DNA/RNA hybrid. With increasing force, the dye binding is more abundant resulting in higher fluorescence signal. Once the force is too high, the tether breaks, and the fluorescence signal is lost (**Figure 8B**). For the experiments with bacterial ribosomes (**Figure 8C**), non-specific labeling of the lysine residues was employed using N-hydroxysuccinimide (NHS) conjugated to a red fluorescent dye. Although there is a risk of decreasing the activity of labeled protein/complex, the big advantage is stronger signal achieved as each ribosome is (on average) labeled by multiple fluorophores. The RNA construct contained a ribosome binding site (RBS) recognized by bacterial ribosomes, which was placed in the 5' proximity of the studied RNA sequence. Upon binding of the ribosomes, the fluorescence signal is observed on the tether. Fluorescence data can be further analyzed using image analysis tools[72], and the results can be combined with the force data, allowing the study of folding transitions.

FIGURE AND TABLE LEGENDS:

Figure 1: Schematic of the OT experiment and possible measurement approaches. (A) Schematic illustrating the optical tweezers experiments with the SARS-CoV-2 frameshifting RNA in the middle. RNA is hybridized to ssDNA handles and immobilized on beads. These are used to exert pulling force on the RNA with a focused laser beam. The force is gradually increased until the RNA is unfolded (bottom). **(B)** Schematic of confocal microscopy combined with optical tweezers to monitor binding of labeled factor to RNA. **(C)** Example constant-force data can be obtained by fixing the force at a constant value over time, which allows to precisely measure dwell time of the conformers. **(D)** Example force-distance (FD) curve obtained from a force-ramp measurement. The unfolding step is observed as a sudden rupture in the FD profile.

Figure 2: A general scheme of OT sample synthesis. (A) Example sequence and predicted secondary structure of the studied SARS-CoV-2 frameshifting RNA employed in the study. **(B)** A vector containing the sequence of interest (SoI) flanked by two handle regions serves as the template for generation of the DNA/RNA construct in 3 PCR reactions. Primers are depicted and numbered in the scheme according to their binding sites in the corresponding PCR. PCR 1 yields the *in vitro* transcription template, which is subsequently used for the *in vitro* transcription (IVT) reaction to generate the long RNA molecule (light blue). PCR 2 yields the 5' handle, which is later 3' labeled with biotin. PCR 3 using the forward primer conjugated to digoxigenin produces the 3' digoxigenin-labeled handle. Finally, the two handles and RNA are annealed to give a DNA/RNA hybrid construct suitable for optical tweezers measurements.

Figure 3: Illustration of different microfluidics channel setups. (A) A scheme of the flow cell with 5- microfluidics channels. **(B)** and **(C)** are the zoom-ins of the red-dashed area of **(A)**. **(B)** A simple 3- channel setup with AD beads and SA beads in channels 1 and 3, respectively. Factor is found in channel 2. This setup is suitable for stable proteins with high affinity, thus low concentration is preferred to ensure low fluorescent background. The bead channels on the side allow fixed tether orientation and quick recruitment of new beads if necessary. **(C)** 4-channel setup with Factor in channel 4. Such an arrangement is particularly advantageous for minimal sample consumption. The measurement can be performed directly in channel 4. Alternatively, to avoid background fluorescence signal, the complex can be formed in channel 4 and then the measurement can be performed in channel 3.

Figure 4: Data analysis workflow for force-ramp experiments. (A) Flowchart of the data analysis workflow. The raw data files are first downsampled and filtered, then steps are marked and the individual states are fitted to the corresponding model. **(B)** The raw data contain considerable amount of noise, which obstruct the identification of unfolding/refolding events. Also, in most of the experiments, the frequency of data gathering is higher than necessary. **(C)** Therefore, downsampling and signal filtration are employed to smoothen the data profile. **(D)** The processed curves are finally fitted to the worm-like chain (WLC) model when the molecule is still in the folded state (before the unfolding event), a combination of a WLC model with a freely-jointed chain (FJC) or a second WLC model when the molecule is in an unfolded state (after the unfolding event).

Figure 5: The effect of cut-off-frequency on data output. While the raw data output might be burdened with signal noise (top), it is crucial to choose proper signal filtration parameters for data analysis. Although proper filtration would help in the identification of folding intermediates (cut-off frequency 0.1, middle), over filtration (cut-off frequency <0.001, bottom) may result in loss of resolution.

Figure 6: Example FD trajectories in the absence and presence of ZAP. (A) Unfolding (pink) and refolding (blue) traces of the SARS-CoV-2 RNA in the absence of ZAP. The sample shows readily refolding with only small hysteresis. **(B)** Unfolding (pink) and refolding (blue) traces of the RNA in the presence of *trans*-factor ZAP (400 nM). The sample shows huge hysteresis, suggesting that the protein binds to the single-stranded RNA and prevents its refolding. **(C)** A bar chart showing

the number of unfolding (pink) and refolding (blue) steps in the absence or presence of ZAP. While the distribution of unfolding steps remains almost unaffected by the presence of ZAP, there is a clear drop in the number of refolding steps with ZAP.

Figure 7: Example constant-force data in the absence and presence of ZAP. (A) Constant-force data obtained at forces ranging between 10 (up) to 13 (bottom) pN showing the shift from fully folded state to fully unfolded state of the SARS-CoV-2 frameshifting RNA element. Each graph includes the position vs. time (left) and a histogram plot (right). **(B)** Constant-force data obtained in the presence of ZAP (400 nM). Upon protein binding, the refolding is impaired. At 10 pN, in contrast to RNA alone, in the presence of ZAP RNA mostly exists the unfolded state. Therefore, a shift in the equilibrium force towards lower forces is indicated. **(C)** The histogram of position data can be analyzed by fitting the data to gaussian functions to yield the relative abundance of each state (derived from the area under the curve for each state).

Figure 8: OT combined with confocal microscopy. (A) An example kymograph of the SYTOX Green labeled tether (left). Note the increase in signal intensity at increasing forces. The black arrow marks the tether breakage event, which leads to loss of signal. Depiction of the tether with dye bound to it (Binding) and after breakage without dye (No signal) (right). **(B)** Example kymograph of specific binding of the ribosome on the mRNA (left). The binding event can be observed as a fluorescence signal on the tethered between the two beads. Depiction of tether without (No signal) and with fluorescence-labeled ribosomes bound (Binding) (right).

Table 1: Pipetting scheme for the PCR to generate the optical tweezers constructs.

Table 2: Pipetting scheme for *in vitro* transcription.

Table 3: Pipetting scheme for 3' end biotin labeling.

Table 4: Pipetting scheme for the annealing of the optical tweezers construct.

DISCUSSION:

Here, we demonstrate the use of fluorescence-coupled optical tweezers to study interactions and dynamic behavior of RNA molecules with various ligands. Below, critical steps and limitations of the present technique are discussed.

Critical steps in the protocol

As for many other methods, the quality of the sample is pivotal to obtain reliable data. Therefore, to obtain the highest possible quality samples, it is worth it to spend time to optimize the procedure for sample preparation. The optimization steps include proper primer design, annealing temperatures, RNA and protein purification steps.

Throughout the experiment use of filtered tips and solutions is crucial in order to maintain RNase-free conditions. In addition, the microfluidics system is kept in bleach when not in use. Before starting measurements, it is important to wash the system properly with sodium thiosulfate and RNase-free water to remove the bleach from the system.

In case the same-sized beads are used throughout the experiment, it is not required to perform force calibration each time. Nevertheless, force calibration checks should be done regularly for the reproducibility of experiments.

Modifications and troubleshooting of the method

Fluorophore stability and photobleaching

A complication during fluorescence measurements is photobleaching. Since the time frame to monitor translation can be extended from seconds to minutes depending on the system, photobleaching during the measurements should be also considered and minimized as much as possible[73]. One option is to employ more stable fluorophores, which are less prone to photobleaching, such as recently introduced quantum dots[49,74,75]. Further stability is also achieved by removing oxygen molecules using an "oxygen scavenger" system, such as glucose oxidase coupled with catalase. Glucose oxidase removes oxygen from the environment by turning it into hydrogen peroxide, which is then decomposed by catalase. Alternative oxygen scavenging systems can also be employed[76,77].

Microfluidics

Maintaining a continuous laminar flow is essential for proper measurements. Most importantly, the system should never run dry. Unfortunately, RBPs or other *trans*-acting factors of interest are often available only in small volumes for the experiments, therefore maintaining continuous flow can be challenging and cost intensive. If air bubbles are introduced into the system during the sample application, manual pressure or ethanol wash is usually sufficient for their removal.

Limitations of the method

Combination of OT with confocal microscopy also brings some limitations. First, the focal plane of the confocal unit must be aligned properly with trap centers to allow proper recording of fluorescence signal. Furthermore, for confocal measurements, handles of at least 2 kb at each site are usually needed[17]. Although in principle using longer handles is possible, one should consider the energy contribution of the handles and the change in the persistence length for the accuracy of data analysis[78]. Another crucial point is the oxygen scavengers, which are used to increase the half-life of the fluorophores, also lead to relatively quick changes in pH of the solutions[76]. These changes can be partially compensated by increasing the concentration of the buffering compound; however, during the measurements, samples should be replenished regularly (every 30-60 min) to ensure consistent conditions through the experiment.

ACKNOWLEDGMENTS:

We thank Anuja Kibe and Jun. Prof. Redmond Smyth for critically reviewing the manuscript. We thank Tatyana Koch for expert technical assistance. We thank Kristyna Pekarkova for the help with recording experimental videos. The work in our laboratory is supported by the Helmholtz Association and funding from the European Research Council (ERC) Grant Nr. 948636 (to NC).

DISCLOSURES:

The authors have nothing to disclose.

REFERENCES:

1 Balcerak, A., Trebinska-Stryjewska, A., Konopinski, R., Wakula, M., Grzybowska, E. A. RNA–protein interactions: disorder, moonlighting and junk contribute to eukaryotic complexity. *Open Biology.* **9** (6), 190096 (2019).

2 Armaos, A., Zacco, E., Sanchez de Groot, N., Tartaglia, G. G. RNA-protein interactions: Central players in coordination of regulatory networks. *BioEssays.* **43** (2), 2000118 (2021).

3 Firth, A. E. & Brierley, I. Non-canonical translation in RNA viruses. *Journal of General Virology.* **93** (Pt 7), 1385-1409 (2012).

4 Caliskan, N., Peske, F., Rodnina, M. V. Changed in translation: mRNA recoding by −1 programmed ribosomal frameshifting. *Trends in Biochemical Sciences.* **40** (5), 265-274 (2015).

5 Jaafar, Z. A., Kieft, J. S. Viral RNA structure-based strategies to manipulate translation. *Nature Reviews Microbiology.* **17** (2), 110-123 (2019).

6 Eswarappa, S. M. et al. Programmed translational readthrough generates antiangiogenic VEGF-Ax. *Cell.* **157** (7), 1605-1618 (2014).

7 Rodnina, M. V. et al. Translational recoding: canonical translation mechanisms reinterpreted. *Nucleic Acids Research.* **48** (3), 1056-1067 (2020).

8 Li, Y. et al. Transactivation of programmed ribosomal frameshifting by a viral protein. *Proceedings of the National Academy of Sciences.* **111** (21), E2172 (2014).

9 Napthine, S. et al. Protein-directed ribosomal frameshifting temporally regulates gene expression. *Nature Communications.* **8** (1), 15582 (2017).

10 Patel, A. et al. Molecular characterization of the RNA-protein complex directing -2/-1 programmed ribosomal frameshifting during arterivirus replicase expression. *Journal of Biological Chemistry.* **295** (52), 17904-17921 (2020).

11 Napthine, S., Bell, S., Hill, C. H., Brierley, I., Firth, A. E. Characterization of the stimulators of protein-directed ribosomal frameshifting in Theiler's murine encephalomyelitis virus. *Nucleic Acids Research.* **47** (15), 8207-8223 (2019).

12 Marshall, R. A., Aitken, C. E., Dorywalska, M., Puglisi, J. D. Translation at the Single-Molecule Level. *Annual Review of Biochemistry.* **77** (1), 177-203 (2008).

13 Rodnina, M. V. The ribosome in action: Tuning of translational efficiency and protein folding. *Protein science : A publication of the Protein Society.* **25** (8), 1390-1406 (2016).

14 Rodnina, M. V., Fischer, N., Maracci, C., Stark, H. Ribosome dynamics during decoding. *Philosophical Transactions of Royal Society of London B Biological Sciences.* **372** (1716) (2017).

15 Yan, S., Wen, J. D., Bustamante, C., Tinoco, I., Jr. Ribosome excursions during mRNA translocation mediate broad branching of frameshift pathways. *Cell.* **160** (5), 870-881 (2015).

16 Liu, T. et al. Direct measurement of the mechanical work during translocation by the ribosome. *eLife.* **3,** e03406-e03406 (2014).

17 Desai, V. P. et al. Co-temporal force and fluorescence measurements reveal a ribosomal gear shift mechanism of translation regulation by structured mRNAs. *Molecular Cell.* **75** (5), 1007-1019.e1005 (2019).
18 Choi, J., O'Loughlin, S., Atkins, J. F., Puglisi, J. D. The energy landscape of -1 ribosomal frameshifting. *Science Advances.* **6** (1), eaax6969 (2020).
19 Prabhakar, A., Puglisi, E. V. & Puglisi, J. D. Single-molecule fluorescence applied to translation. *Cold Spring Harbor Perspectives in Biology.* **11** (1), a032714, (2019).
20 Bao, C. et al. mRNA stem-loops can pause the ribosome by hindering A-site tRNA binding. *Elife.* **9**, e55799, (2020).
21 Chen, J., Tsai, A., O'Leary, S. E., Petrov, A., Puglisi, J. D. Unraveling the dynamics of ribosome translocation. *Current Opinion in Structural Biology.* **22** (6), 804-814 (2012).
22 Qu, X. et al. The ribosome uses two active mechanisms to unwind messenger RNA during translation. *Nature.* **475** (7354), 118-121 (2011).
23 Zheng, Q. et al. Ultra-stable organic fluorophores for single-molecule research. *Chemical Society Reviews.* **43** (4), 1044-1056 (2014).
24 Blanchard, S. C. Single-molecule observations of ribosome function. *Current Opinion in Structural Biology.* **19** (1), 103-109 (2009).
25 Juette, M. F. et al. The bright future of single-molecule fluorescence imaging. *Current Opinion in Chemical Biology.* **20,** 103-111(2014).
26 McCauley, M. J., Williams, M. C. Mechanisms of DNA binding determined in optical tweezers experiments. *Biopolymers.* **85** (2), 154-168 (2007).
27 Ashkin, A., Dziedzic, J. M., Bjorkholm, J. E., Chu, S. Observation of a single-beam gradient force optical trap for dielectric particles. *Optics Letters.* **11** (5), 288-290 (1986).
28 Bustamante, C., Smith, S. B., Liphardt, J. & Smith, D. Single-molecule studies of DNA mechanics. *Current Opinion in Structural Biology.* **10** (3), 279-285 (2000).
29 Choudhary, D., Mossa, A., Jadhav, M., Cecconi, C. Bio-molecular applications of recent developments in optical tweezers. *Biomolecules.* **9** (1), 23 (2019).
30 Moffitt, J. R., Chemla, Y. R., Smith, S. B., Bustamante, C. Recent advances in optical tweezers. *Annual Reviews of Biochemistry.* **77,** 205-228 (2008).
31 Li, P. T. X., Vieregg, J., Tinoco, I. How RNA Unfolds and Refolds. *Annual Review of Biochemistry.* **77** (1), 77-100 (2008).
32 Stephenson, W., Wan, G., Tenenbaum, S. A., Li, P. T. Nanomanipulation of single RNA molecules by optical tweezers. *Journal of Visualized Experiments.* (90), e51542, (2014).
33 Halma, M. T. J., Ritchie, D. B., Cappellano, T. R., Neupane, K., Woodside, M. T. Complex dynamics under tension in a high-efficiency frameshift stimulatory structure. *Proceedings of the National Academy of Sciences.* **116** (39), 19500 (2019).
34 Hansen, T. M., Reihani, S. N. S., Oddershede, L. B., Sørensen, M. A. Correlation between mechanical strength of messenger RNA pseudoknots and ribosomal frameshifting. *Proceedings of the National Academy of Sciences of the United States of America.* **104** (14), 5830-5835 (2007).
35 Zhong, Z. et al. Mechanical unfolding kinetics of the SRV-1 gag-pro mRNA pseudoknot: possible implications for -1 ribosomal frameshifting stimulation. *Science Reports.* **6**, 39549 (2016).

36 McCauley, M. J., Rouzina, I., Li, J., Núñez, M. E., Williams, M. C. Significant differences in RNA structure destabilization by HIV-1 GagDp6 and NCp7 proteins. *Viruses.* **12** (5), 484, doi:10.3390/v12050484 (2020).

37 de Messieres, M. et al. Single-molecule measurements of the CCR5 mRNA unfolding pathways. *Biophysics Journal.* **106** (1), 244-252 (2014).

38 Yang, L. et al. Single-molecule mechanical folding and unfolding of RNA hairpins: Effects of single A-U to A·C pair substitutions and single proton binding and implications for mRNA structure-induced -1 ribosomal frameshifting. *Journal of American Chemical Society.* **140** (26), 8172-8184 (2018).

39 McCauley, M. J. et al. Targeted binding of nucleocapsid protein transforms the folding landscape of HIV-1 TAR RNA. *Proceedings of the National Academy of Sciences of the United States of America.* **112** (44), 13555-13560 (2015).

40 Whitley, K. D., Comstock, M. J., Chemla, Y. R. High-resolution "Fleezers": Dual-trap optical tweezers combined with single-molecule fluorescence detection. *Methods in Molecular Biology (Clifton, N.J.).* **1486**, 183-256 (2017).

41 Yerramilli, V. S., Kim, K. H. Labeling RNAs in live cells using malachite green aptamer scaffolds as fluorescent probes. *ACS Synthetic Biology.* **7** (3), 758-766 (2018).

42 Gross, P., Farge, G., Peterman, E. J., Wuite, G. J. Combining optical tweezers, single-molecule fluorescence microscopy, and microfluidics for studies of DNA-protein interactions. *Methods in Enzymology.* **475**, 427-453 (2010).

43 Zimmer, M. M. et al. The short isoform of the host antiviral protein ZAP acts as an inhibitor of SARS-CoV-2 programmed ribosomal frameshifting. *Nature Communications.* **12** (1), 7193 (2021).

44 Neupane, K., Yu, H., Foster, D. A. N., Wang, F., Woodside, M. T. Single-molecule force spectroscopy of the add adenine riboswitch relates folding to regulatory mechanism. *Nucleic acids research.* **39** (17), 7677-7687 (2011).

45 Ritchie, D. B., Soong, J., Sikkema, W. K., Woodside, M. T. Anti-frameshifting ligand reduces the conformational plasticity of the SARS virus pseudoknot. *Journal of the American Chemical Society.* **136** (6), 2196-2199 (2014).

46 Janissen, R. et al. Invincible DNA tethers: covalent DNA anchoring for enhanced temporal and force stability in magnetic tweezers experiments. *Nucleic Acids Research.* **42** (18), e137-e137 (2014).

47 Smith, S. B., Cui, Y., Bustamante, C. Overstretching B-DNA: The elastic response of individual double-stranded and single-stranded DNA molecules. *Science.* **271** (5250), 795 (1996).

48 Puljung, M. C., Zagotta, W. N. Labeling of specific cysteines in proteins using reversible metal protection. *Biophysical Journal.* **100** (10), 2513-2521 (2011).

49 Toseland, C. P. Fluorescent labeling and modification of proteins. *Journal of Chemical Biology.* **6** (3), 85-95 (2013).

50 Hill, C. H. et al. Structural and molecular basis for Cardiovirus 2A protein as a viral gene expression switch. *Nature Communications.* **12** (1), 7166 (2021).

51 Butterworth, S. On the theory of filter amplifiers. *Experimental Wireless and the Wireless Engineer.* **7,** 536-541 (1930).

52 Wang, M. D., Yin, H., Landick, R., Gelles, J., Block, S. M. Stretching DNA with optical tweezers. *Biophysics Journal.* **72** (3), 1335-1346 (1997).
53 Mukhortava, A. et al. Structural heterogeneity of attC integron recombination sites revealed by optical tweezers. *Nucleic Acids Research.* **47** (4), 1861-1870 (2019).
54 Buck, S., Pekarek, L., Caliskan, N. POTATO: An automated pipeline for batch analysis of optical tweezers data. *bioRxiv.* 2021.2011.2011.468103 (2021).
55 Zhang, Y., Jiao, J. & Rebane, A. A. Hidden Markov modeling with detailed balance and its application to single protein folding. *Biophysical Journal.* **111** (10), 2110-2124 (2016).
56 Sgouralis, I., Pressé, S. An introduction to infinite HMMs for single-molecule data analysis. *Biophysics Journal.* **112** (10), 2021-2029 (2017).
57 Müllner, F. E., Syed, S., Selvin, P. R., Sigworth, F. J. Improved hidden Markov models for molecular motors, part 1: basic theory. *Biophysical Journal.* **99** (11), 3684-3695 (2010).
58 Elms, P. J., Chodera, J. D., Bustamante, C. J., Marqusee, S. Limitations of constant-force-feedback experiments. *Biophysical Journal.* **103** (7), 1490-1499 (2012).
59 Re, A., Joshi, T., Kulberkyte, E., Morris, Q., Workman, C. T. RNA-protein interactions: an overview. *Methods Molecular Biology.* **1097**, 491-521 (2014).
60 Jankowsky, E., Harris, M. E. Specificity and nonspecificity in RNA-protein interactions. *Nature reviews. Molecular Cell Biology.* **16** (9), 533-544 (2015).
61 Lim, F., Peabody, D. S. RNA recognition site of PP7 coat protein. *Nucleic Acids Research.* **30** (19), 4138-4144 (2002).
62 Sunbul, M., Jäschke, A. SRB-2: a promiscuous rainbow aptamer for live-cell RNA imaging. *Nucleic Acids Research.* **46** (18), e110-e110 (2018).
63 Sanchez de Groot, N. et al. RNA structure drives interaction with proteins. *Nature Communications.* **10** (1), 3246 (2019).
64 Zeffman, A., Hassard, S., Varani, G., Lever, A. The major HIV-1 packaging signal is an extended bulged stem loop whose structure is altered on interaction with the Gag polyprotein. *Journal of Molecular Biology.* **297** (4), 877-893 (2000).
65 Mangeol, P. et al. Probing ribosomal protein–RNA interactions with an external force. *Proceedings of the National Academy of Sciences.* **108** (45), 18272 (2011).
66 Luo, X. et al. Molecular mechanism of RNA recognition by Zinc-Finger antiviral protein. *Cell Reports.* **30** (1), 46-52.e44 (2020).
67 Qu, X., Lancaster, L., Noller, H. F., Bustamante, C., Tinoco, I., Jr. Ribosomal protein S1 unwinds double-stranded RNA in multiple steps. *Proceedings of the National Academy of Science U. S. A.* **109** (36), 14458-14463 (2012).
68 Chandra, V., Hannan, Z., Xu, H., Mandal, M. Single-molecule analysis reveals multi-state folding of a guanine riboswitch. *Nature Chemical Biology.* **13** (2), 194-201 (2017).
69 Savinov, A., Perez, C. F., Block, S. M. Single-molecule studies of riboswitch folding. *Biochimica et Biophysica Acta.* **1839** (10), 1030-1045 (2014).
70 Kelly, J. A. et al. Structural and functional conservation of the programmed ribosomal frameshift signal of SARS coronavirus 2 (SARS-CoV-2). *Journal of Biological Chemistry.* **295** (31), 10741-10748 (2020).
71 Neupane, K. et al. Structural dynamics of single SARS-CoV-2 pseudoknot molecules reveal topologically distinct conformers. *Nature Communications.* **12** (1), 4749 (2021).

72 Schindelin, J. et al. Fiji: an open-source platform for biological-image analysis. *Nature Methods.* **9** (7), 676-682 (2012).

73 Zheng, Q., Jockusch, S., Zhou, Z., Blanchard, S. C. The contribution of reactive oxygen species to the photobleaching of organic fluorophores. *Photochemistry and Photobiology.* **90** (2), 448-454 (2014).

74 Deerinck, T. J. The application of fluorescent quantum dots to confocal, multiphoton, and electron microscopic imaging. *Toxicologic Pathology.* **36** (1), 112-116 (2008).

75 Rill, N., Mukhortava, A., Lorenz, S., Tessmer, I. Alkyltransferase-like protein clusters scan DNA rapidly over long distances and recruit NER to alkyl-DNA lesions. *Proceedings of the National Academy of Science U. S. A.* **117** (17), 9318-9328 (2020).

76 Swoboda, M. et al. Enzymatic oxygen scavenging for photostability without pH drop in single-molecule experiments. *ACS Nano.* **6** (7), 6364-6369 (2012).

77 Aitken, C. E., Marshall, R. A., Puglisi, J. D. An oxygen scavenging system for improvement of dye stability in single-molecule fluorescence experiments. *Biophysical Journal.* **94** (5), 1826-1835 (2008).

78 Wen, J.-D. et al. Force unfolding kinetics of RNA using optical tweezers. I. Effects of experimental variables on measured results. *Biophysical journal.* **92** (9), 2996-3009 (2007).

Figure_1

Click here to access/download;Figure;Figure_01.pdf

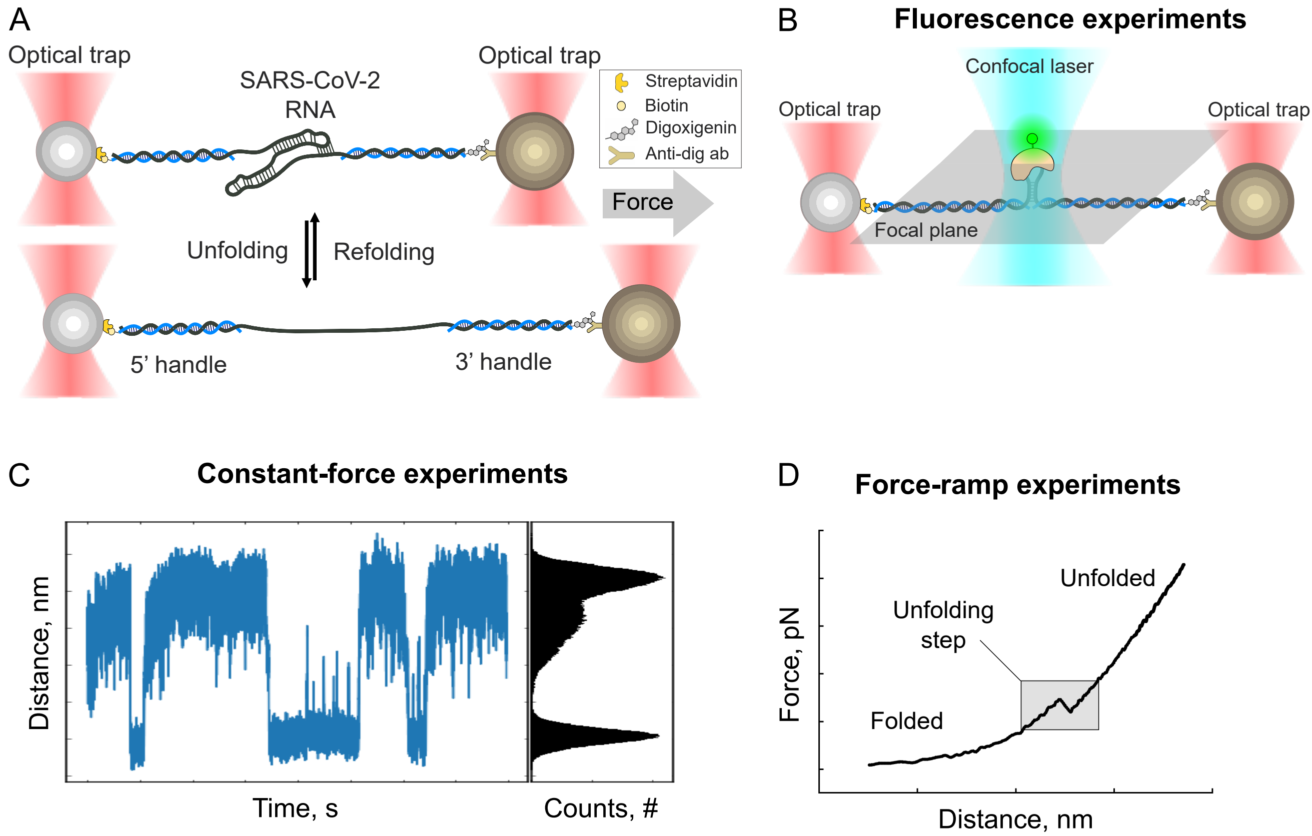

Figure_2

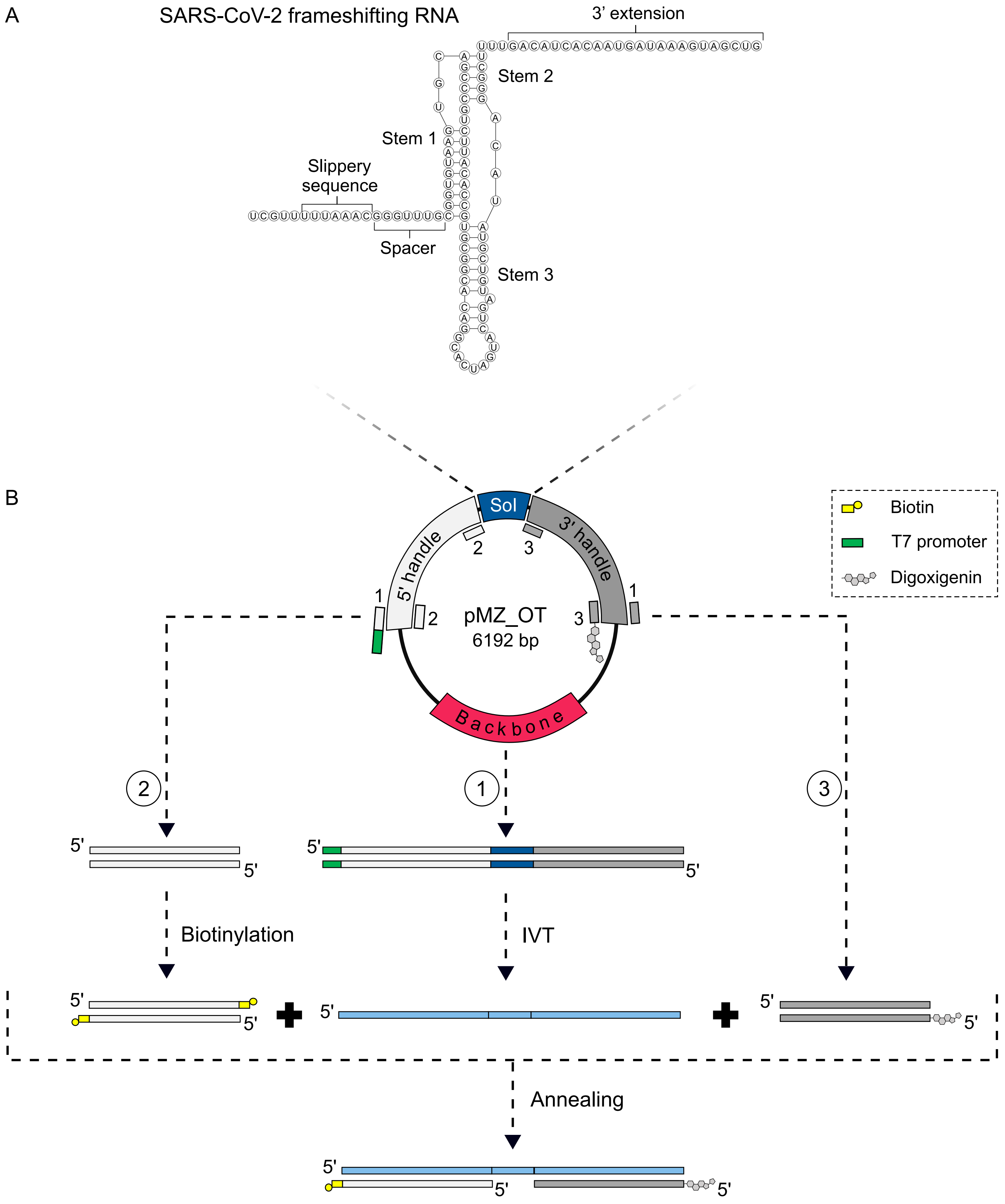
A
SARS-CoV-2 frameshifting RNA
3' extension
Stem 1
Stem 2
Stem 3
Slippery sequence
Spacer
B
Biotin
T7 promoter
Digoxigenin
Sol
5' handle
3' handle
pMZ_OT
6192 bp
Backbone
Biotinylation
IVT
Annealing

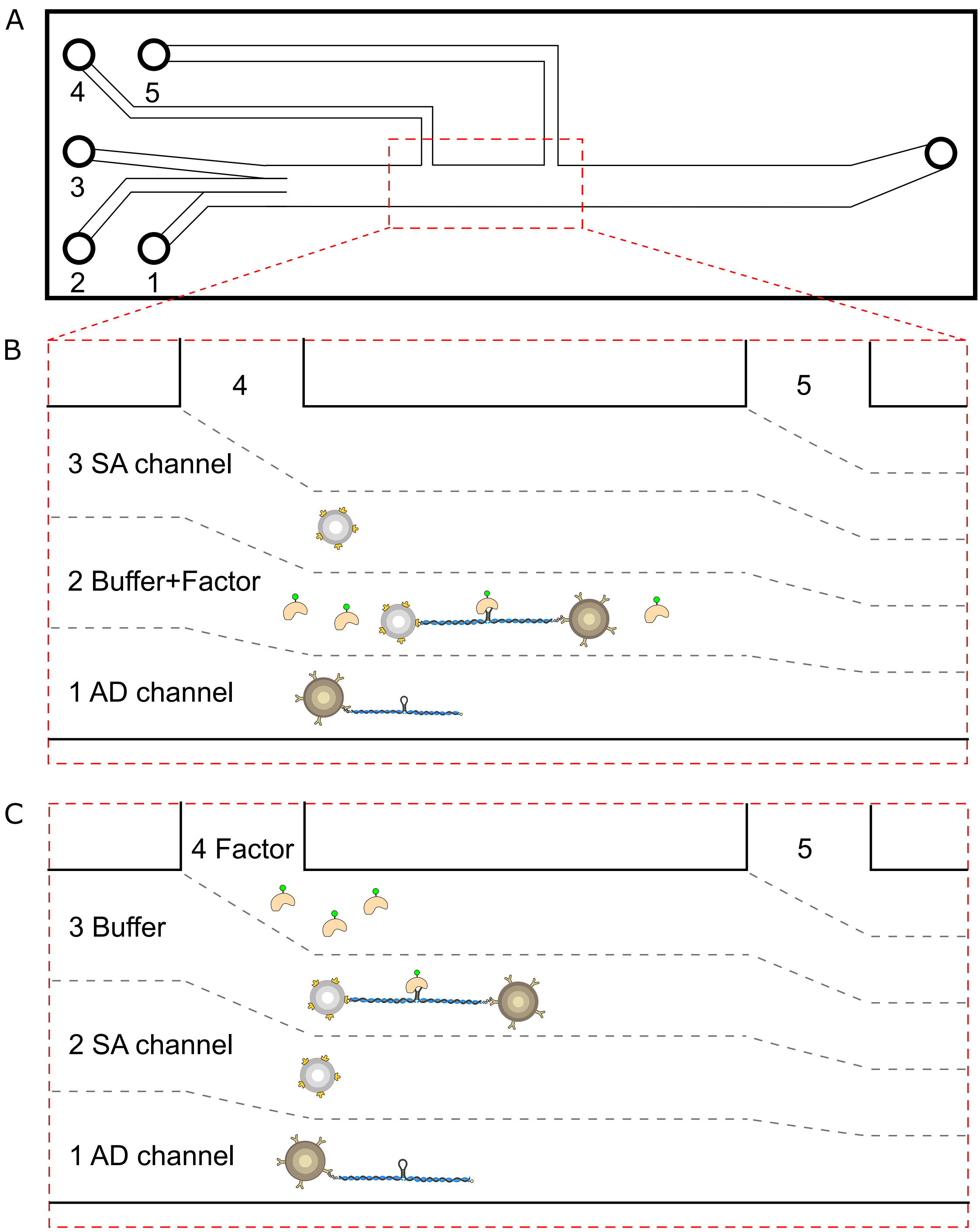
A
4
5
3
2
1
B
4
5
3 SA channel
2 Buffer+Factor
1 AD channel
C
4 Factor
5
3 Buffer
2 SA channel
1 AD channel

Figure_4

Click here to access/download;Figure;Figure_04.pdf

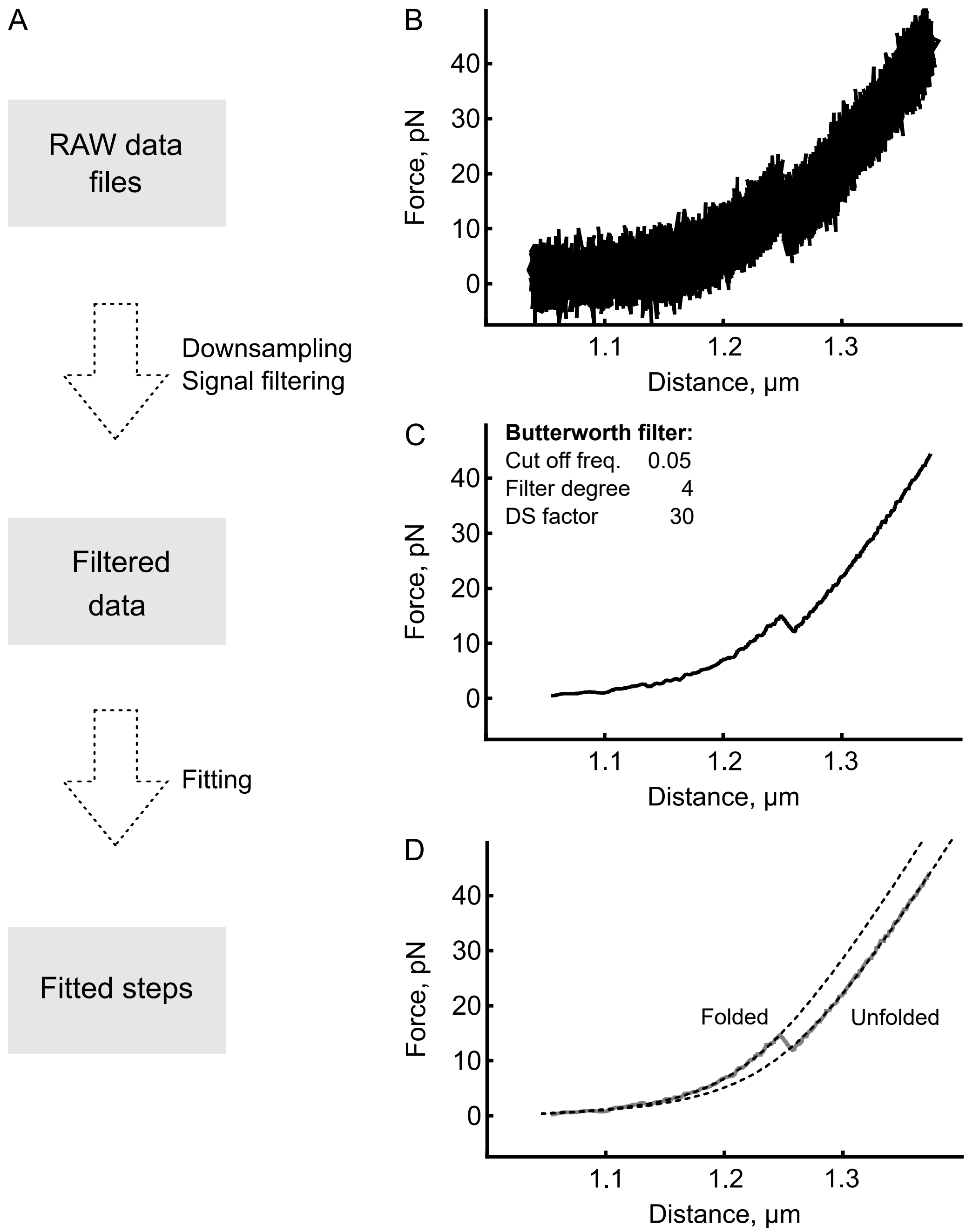

Figure_5

Click here to access/download;Figure;Figure_05.pdf

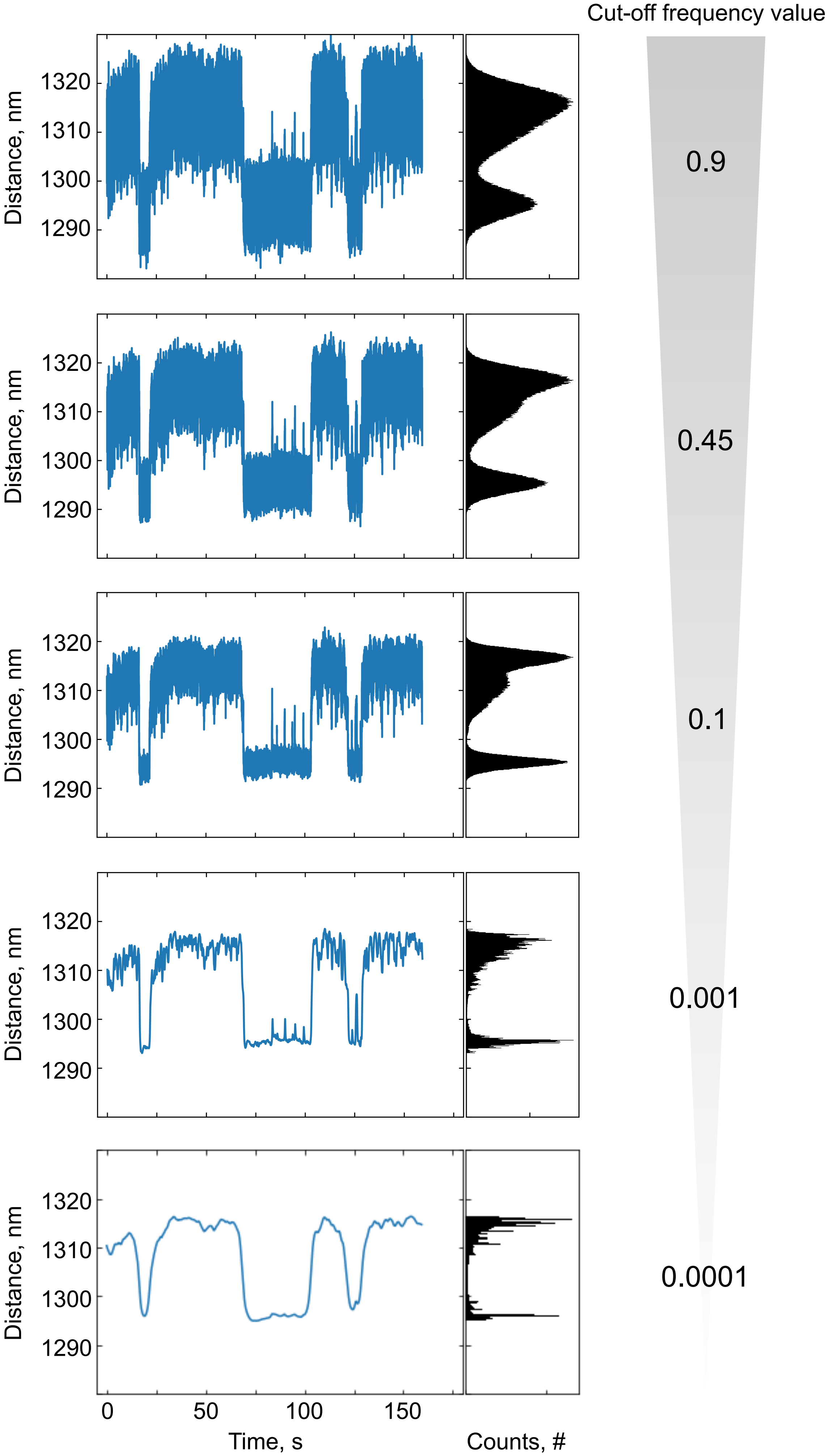

Figure_6

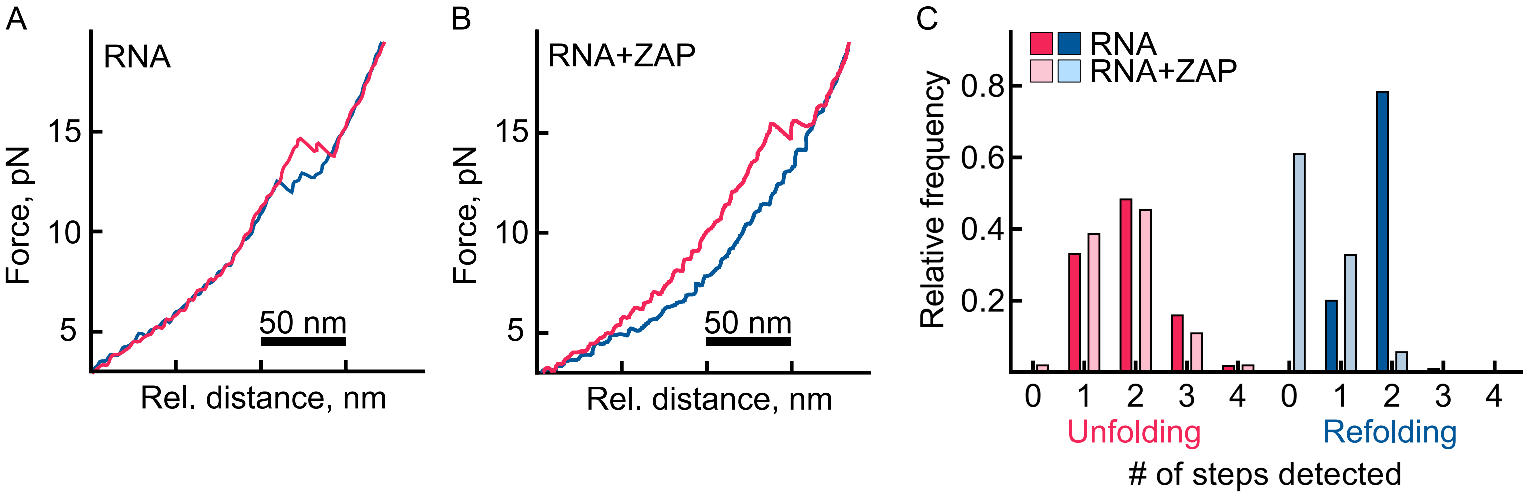
A
RNA
Force, pN
5
10
15
50 nm
Rel. distance, nm
B
RNA+ZAP
Force, pN
5
10
15
50 nm
Rel. distance, nm
C
RNA
RNA+ZAP
Relative frequency
0.2
0.4
0.6
0.8
0 1 2 3 4 0 1 2 3 4
Unfolding
Refolding
# of steps detected

Figure_7

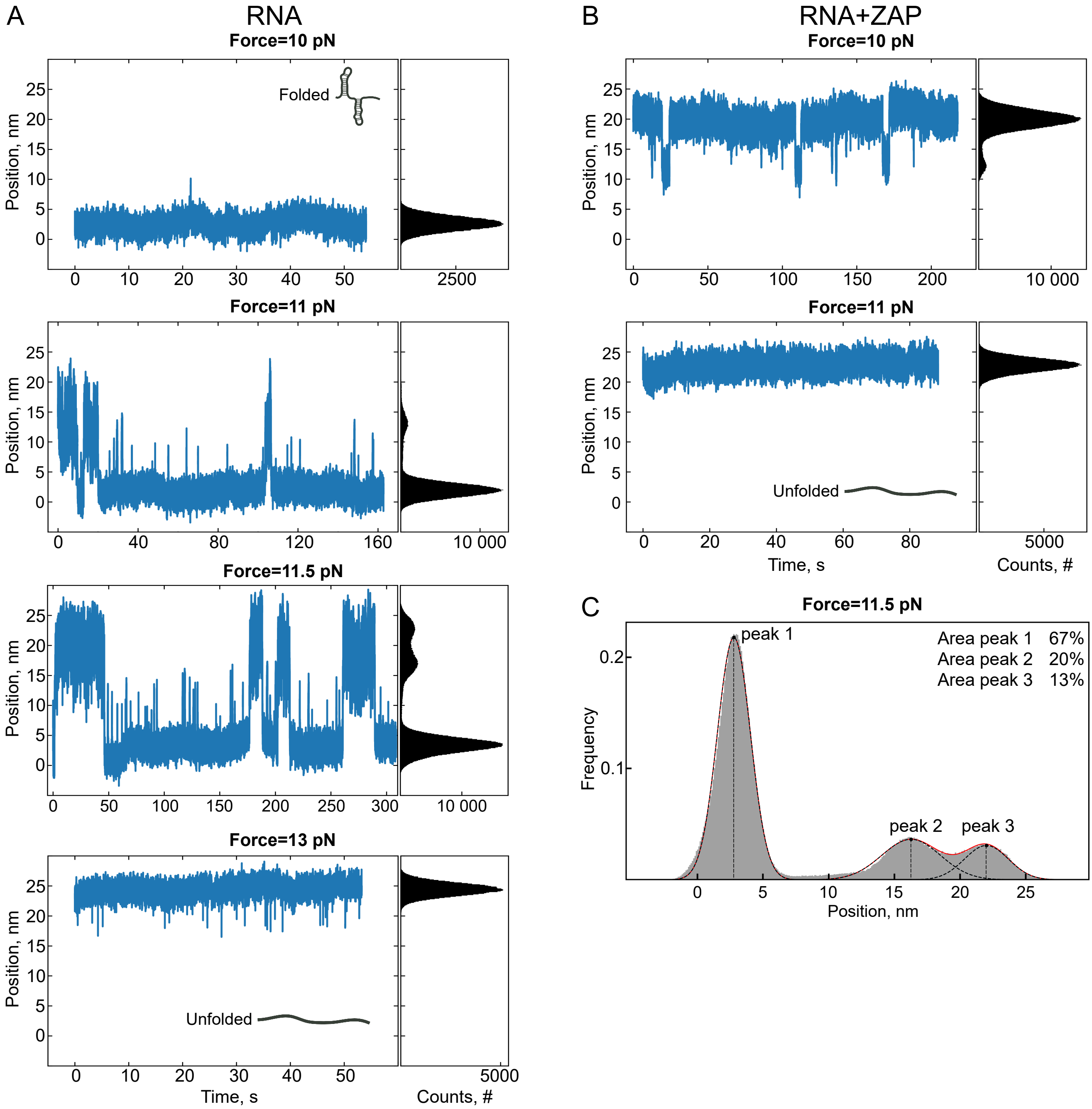

A
RNA
Force=10 pN
Folded
Position, nm
2500
Force=11 pN
10 000
Force=11.5 pN
10 000
Force=13 pN
Unfolded
Time, s
5000
Counts, #
B
RNA+ZAP
Force=10 pN
10 000
Force=11 pN
Unfolded
5000
C
Force=11.5 pN
peak 1
peak 2
peak 3
Area peak 1 67%
Area peak 2 20%
Area peak 3 13%
Frequency
Position, nm

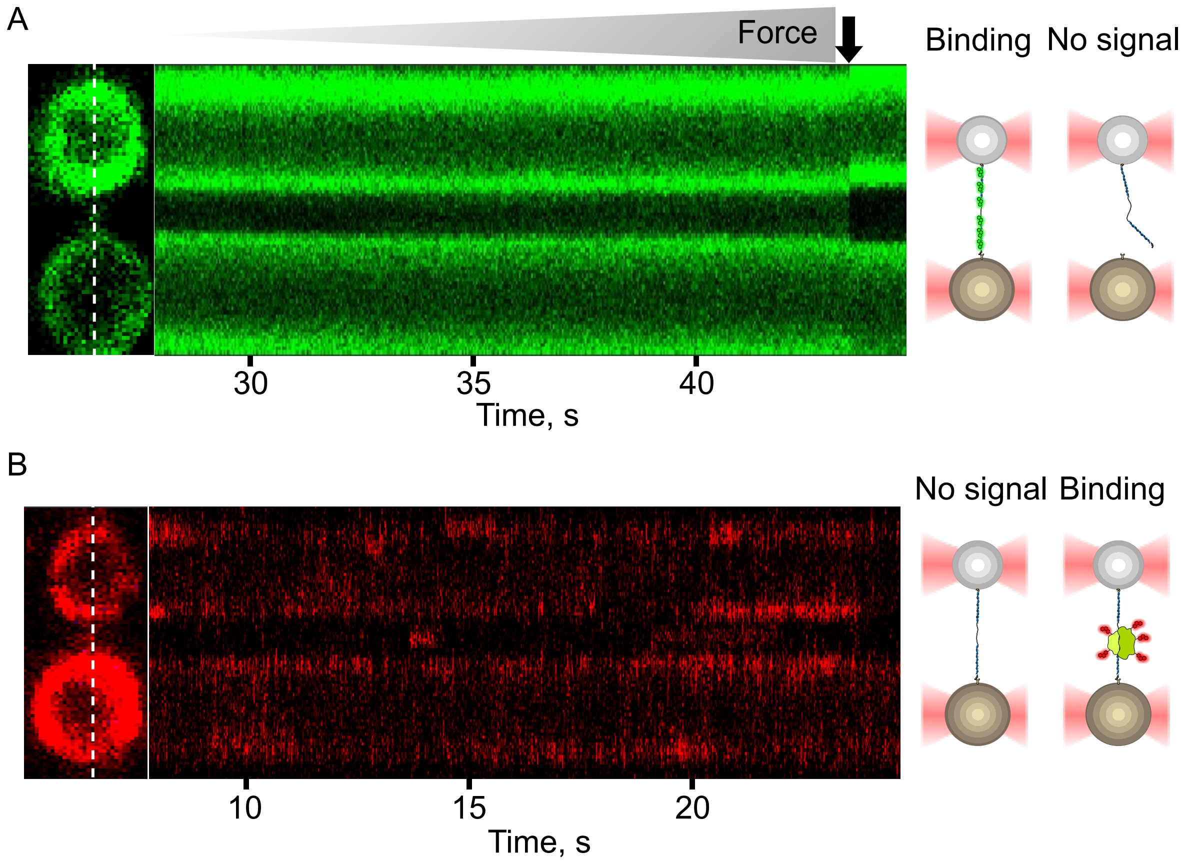
A
Force
Binding
No signal
30
35
40
Time, s
B
No signal
Binding
10
15
20
Time, s

	Stock concentration	Final concentration	Volume
Reaction volume	-	-	500 µL
10× buffer	10×	1×	50 µL
dNTP mix	10 mM	0.2 mM	10 µL
High fidelity DNA polymerase	1.25 U/µL	0.025 U/µL	10 µL
Primer 1	10 µM	0.4 µM	20 µL
Primer 2	10 µM	0.4 µM	20 µL
Template	100 ng/µL	1 ng/µL	5 µL
Water	-	-	385 µL

Table_2

Click here to access/download;Table;Table_02.xlsx

	Stock concentration	Final concentration	Volume
Reaction volume	-	-	300 µL
5× buffer	5×	1×	60 µL
rNTP mix	25 mM	5 mM	60 µL
RNase inhibitor	40 U/µL	0.7 U/µL	5 µL
Pyrophosphatase	100 U/mL	1.7 mU/µL	4 µL
DTT	100 mM	3.3 mM	10 µL
T7 RNA polymerase	50 U/µL	3.3 U/µL	20 µL
Template	120 ng/µL	2 ng/µL	5 µL
Water	-	-	136 µL

	Stock concentration	Final concentration	Volume
Reaction volume	-	-	100 µL
10× buffer (NEB 2.1)	10×	1×	10 µL
BSA	1 µg/ml	100 ng/µL	1 µL
Biotin-16-dUTP	1 mM	50 µM	5 µL
T4 DNA polymerase	30 U/µL	1.5 U/µL	5 µL
DNA 5’ handle (20-60 µg)	300 ng/µL	237 ng/µL	79 µL

	Stock concentration	Final concentration	Final amount	Volume
Reaction volume	-	-	-	300 µL
Annealing buffer	1.25×	1×	-	240 µL
Rnase inhibitors	40 U/µL	0.5 U/µL	-	5 µL
5' biotinylated DNA handle	300 ng/µL	10 ng/µL	3 µg	10 µL
3' DNA handle	300 ng/µL	10 ng/µL	3 µg	10 µL
RNA	150 ng/µL	10 ng/µL	3 µg	20 µL
Water	-	-	-	5 µL

Click here to access/download
Table of Materials
JoVE_Materials_rev.xls

HIRI HELMHOLTZ
Institute for RNA-based Infection Research

Helmholtz Institute for RNA-based Infection Research | Dept. REMI
Josef-Schneider-Str. 2 | D 15 | 97080 Würzburg | Germany

Dr. Vineeta Bajaj

Dr. Nam Nguyen

Review Editors

JoVE

Jun. Prof. Dr. Neva Caliskan
Group leader
Recoding Mechanisms in Infections
Tel. 0931 31-85298
Fax 0931 31-82578
neva.caliskan@ helmholtz-hiri.de

Revisions for JoVE62589 04.08.2021

Dear Editors,

We thank you and the reviewers for the valuable comments on the manuscript. We have edited the manuscript to address these concerns and suggestions.

Along with the revised manuscript please find the detailed point by point response for the manuscript entitled “Optical Tweezers to Study RNA-Protein Interactions in Translation Regulation” below.

We believe that the manuscript is now suitable for publication in *JoVE.*

Sincerely yours,

Dr. Neva Caliskan

Helmholtz Institute for RNA-based Infection Research (HIRI)
Josef-Schneider-Str. 2
97080 Würzburg
Germany
Phone +49 931 31-89235
Fax +49 931 31-82578
www.helmholtz-hiri.de

Registered Office:
Helmholtz-Zentrum
für Infektionsforschung GmbH
Inhoffenstraße 7
38124 Braunschweig

Chair of Supervisory Board:
MinDir'in Prof. Veronika von Messling,
Federal Ministry of Education and Research

Scientific Director:
Prof. Dirk Heinz

Administrative Director:
Silke Tannapfel

Registry Court:
Amtsgericht Braunschweig HRB 477
VAT Reg. No DE 11 48 15 244

St.-Nr. 13/200/24006

An institution of
HZI HELMHOLTZ Centre for Infection Research

In cooperation with
Julius-Maximilians-UNIVERSITÄT WÜRZBURG

Editorial comments:

Changes to be made by the Author(s):

1. As the sample preparation in step 1 of the protocol is not the focus of the experiment, please add more details here by citing previous publications: cloning reference, PCR reference, transcription reference, labeling reference, etc.

- Thank you for these suggestions. We now added more references to make it easier for the reader to find the detailed information. Namely:
    - Halma, M. T. J., Ritchie, D. B., Cappellano, T. R., Neupane, K. & Woodside, M. T. Complex dynamics under tension in a high-efficiency frameshift stimulatory structure. *Proceedings of the National Academy of Sciences.* **116** (39), 19500, doi:10.1073/pnas.1905258116, (2019).
    - Zimmer, M. M. et al. Revealing the host antiviral protein ZAP-S as an inhibitor of SARS-CoV-2 programmed ribosomal frameshifting. bioRxiv. 2021.2005.2031.445667, doi:10.1101/2021.05.31.445667, (2021).
    - Hill, C. H. et al. Structural and molecular basis for Cardiovirus 2A protein as a viral gene expression switch. bioRxiv. 2020.2008.2011.245035, doi:10.1101/2020.08.11.245035, (2021).
    - Stephenson, W., Wan, G., Tenenbaum, S. A. & Li, P. T. Nanomanipulation of single RNA molecules by optical tweezers. J Vis Exp. (90), doi:10.3791/51542, (2014).

2. We have a note saying to withhold acceptance until the parent publication is published. Is the parent publication published? Do you want us to withhold acceptance or publication of this article until the parent publication is published?

- Yes, we would like to withhold the process until our parent publication is published (currently under revision in Nature Communications).

Changes to be made by the Author(s) regarding the video:

1. Audio

Interview audio it too low and needs to be raised by 6dbs.

- We thank the editors for pointing this out to us. We increased the audio volume of the interview parts to match better with the volume of narrative.

2. Pacing

There are a bunch dip to blacks that occur when there should be either cross dissolves or dip to white. Please remove the dips to black and use a cross dissolve instead at these time points: 03:23, 03:36, 04:52, 05:00, 05:08, 05:18, 05:19, 07:14, 07:31, 08:04, 10:05, 10:12

- Changed.

Please dip to white at these time points instead of black for the section titles: 04:18, 04:22, 05:47, 05:49, 09:18, 09:22, 12:18

- We thank editors. In the previous editorial comments we were instructed to use cross dissolves together with dips to black, now we change the dips to black to dips to white.

05:41 and 07:25 - These shots go on too long. Please shorten so we can get to the next shot sooner.

- We thank the editors for pointing this out. We shortened the video accordingly.

3. Composition

The intro and outro title cards and the results section all have branding on the bottom of the frame. Please remove any sort of branding such as university logos.

- The logo is now removed.

1:58 - Please include a protocol title card.

- We thank the editors for this suggestion. We now renamed the “timeline” to “protocol” and put the representative results separately.

04:05 - This shot looks like there's a stabilization effect happening, which is making the image look wobbly. Please remove this effect.

- We tried to adjust the cutting and speed of the video in order to remove this effect.

4. 2:25/6:26 - Table 1: Please use SI abbreviations for time. Please capitalize the L in the microliter abbreviation.

- Table 1 does not include time units. The only time “time” units were used is description of sample preparation (06:15-06:29). Since the incubation period is between 10 to 20 minutes, we used “min” as the universally accepted abbreviation. We find use of seconds (SI unit) confusing.
- All “liter” abbreviations are now capitalized.